The intracellular environment affects protein–protein interactions

Shannon L. Speer[a,1], Wenwen Zheng[b,c,1], Xin Jiang[b,c], I-Te Chu[a], Alex J. Guseman[a], Maili Liu[b], Gary J. Pielak[a,d,e,f,2], and Conggang Li[b,2]

[a]Department of Chemistry, University of North Carolina, Chapel Hill, NC 27599; [b]Key Laboratory of Magnetic Resonance in Biological Systems, State Key Laboratory of Magnetic Resonance and Atomic and Molecular Physics, National Center for Magnetic Resonance in Wuhan, Wuhan National Laboratory for Optoelectronics, Wuhan Institute of Physics and Mathematics, Innovation Academy for Precision Measurement Science and Technology, Chinese Academy of Sciences, 430071 Wuhan, China; [c]Graduate University of Chinese Academy of Sciences, 100049 Beijing, China; [d]Department of Biochemistry and Biophysics, University of North Carolina, Chapel Hill, NC 27599; [e]Lineberger Comprehensive Cancer Center, University of North Carolina, Chapel Hill, NC 27599; and [f]Integrative Program for Biological and Genome Sciences, University of North Carolina, Chapel Hill, NC 27599

Edited by Martin Gruebele, University of Illinois at Urbana–Champaign, Urbana, IL, and approved January 8, 2021 (received for review September 23, 2020)

Protein–protein interactions are essential for life but rarely thermodynamically quantified in living cells. In vitro efforts show that protein complex stability is modulated by high concentrations of cosolutes, including synthetic polymers, proteins, and cell lysates via a combination of hard-core repulsions and chemical interactions. We quantified the stability of a model protein complex, the A34F GB1 homodimer, in buffer, *Escherichia coli* cells and *Xenopus laevis* oocytes. The complex is more stable in cells than in buffer and more stable in oocytes than *E. coli*. Studies of several variants show that increasing the negative charge on the homodimer surface increases stability in cells. These data, taken together with the fact that oocytes are less crowded than *E. coli* cells, lead to the conclusion that chemical interactions are more important than hard-core repulsions under physiological conditions, a conclusion also gleaned from studies of protein stability in cells. Our studies have implications for understanding how promiscuous—and specific—interactions coherently evolve for a protein to properly function in the crowded cellular environment.

macromolecular crowding | protein | protein–protein interactions | thermodynamics

Proteins rarely work alone. Networks of protein–protein interactions turn a myriad of chemical signals into physiological responses that maintain intracellular homeostasis (1). Therefore, it is unsurprising that nearly two-thirds of disease-causing missense mutations involve protein complexes (2). However, nearly all equilibrium thermodynamic and kinetic studies of protein–protein interactions have been performed in dilute buffer. Acquiring quantitative equilibrium data on protein complexes in cells, despite the fact that living things are not at equilibrium, is important for two reasons. First, the equilibrium condition is the starting point for estimating the driving force under nonequilibrium conditions (3). Second, recent results on protein stability show that conclusions from experiments conducted in dilute solution cannot be extrapolated to the crowded and complex intracellular environment (4).

The cellular interior contains a variety of proteins, nucleic acids, and small molecules. In the bacterium *Escherichia coli*, the concentration of macromolecules can exceed 300 g/L and occupy up to 30% of volume (5). The macromolecule concentration in eukaryotic cells is smaller (6) but still hundreds of times larger than the solute concentrations used in most in vitro studies. Furthermore, the majority of proteins in the cells studied here, *E. coli* and oocytes, are net polyanions with mean isoelectric points of 6.6 and 6.7, respectively (7). Understanding how the intracellular environment modulates protein—and protein complex—stability is important because the totality of weak interactions in cells form the so-called quinary structure that organizes the crowded cellular interior (8–10). Importantly, these interactions cannot be measured in dilute solutions.

The physical consequences of macromolecular crowding arise from two components: hard-core repulsions and so-called "soft" chemical interactions (11). Hard-core repulsion is a steric effect, arising from the impenetrable nature of atoms. Steric repulsions reduce the volume available to reactants and products. Simple theory predicts that sterics favor compact states (12). For small, folded proteins, stability is described by the two-state equilibrium between the biologically active folded state and the inactive, higher-energy, and less-compact unfolded state (13). For protein complex formation involving folded proteins, which comprises an equilibrium between constituent proteins and the complex, the complex exposes less surface than the sum of the two monomers (14). Thus, simple theory predicts stabilization of proteins and protein complexes, although more sophisticated theoretical efforts focused on the size of crowding molecule predict stabilization or destabilization (15, 16).

Soft interactions include hydrogen bonds and charge–charge, water–protein, solute–protein, and hydrophobic interactions. Of these, the only strong repulsive interaction is that from the opposition of like charges. These repulsions add to the hard-core effect and are therefore stabilizing. The other soft interactions are attractive and destabilizing because they favor expanded conformations that allow access to the attractive surfaces.

Until recently the focus was on hard-core interactions and crowding (17) because studies of protein stability (quantified as

Significance

Protein–protein interactions are essential for proper cellular function. Macromolecular crowding can influence these interactions via two phenomena: hard-core repulsions and soft (chemical) interactions. Simple theory predicts that hard-core repulsions are stabilizing, and stabilization increases with increased crowding, while chemical interactions can be stabilizing or destabilizing. We investigated the effect of the cellular environment on a model protein–protein interaction in a prokaryote (*Escherichia coli*) and a eukaryote (*Xenopus laevis* oocytes). The observation that the complex is more stable in the eukaryote, even though it is less crowded, highlights the key role played by chemical interactions under physiologically relevant conditions.

Author contributions: S.L.S., W.Z., X.J., I.-T.C., A.J.G., M.L., G.J.P., and C.L. designed research; S.L.S., W.Z., X.J., and I.-T.C. performed research; S.L.S., W.Z., X.J., I.-T.C., A.J.G., G.J.P., and C.L. analyzed data; S.L.S., W.Z., X.J., I.-T.C., A.J.G., M.L., G.J.P., and C.L. wrote the paper; and G.J.P. supervised the group.

The authors declare no competing interest.

This article is a PNAS Direct Submission.

[1]S.L.S. and W.Z. contributed equally to this work.

[2]To whom correspondence may be addressed. Email: gary_pielak@unc.edu or conggangli@wipm.ac.cn.

This article contains supporting information online at https://www.pnas.org/lookup/suppl/doi:10.1073/pnas.2019918118/-/DCSupplemental.

Published March 8, 2021.

the free energy of unfolding, $\Delta G_U^{o'}$) in uncharged synthetic polymers tended to show only a stabilizing influence compared to buffer alone (11). However, recent studies of stability under more physiologically relevant crowded conditions and in living cells show, by and large, a decrease in stability (4). Studies of protein–protein interactions in vitro under physiologically relevant crowded conditions also show the importance of chemical interactions (18, 19).

Yeast two-hybrid techniques, coimmunoprecipitation, and split systems provide simple yes/no information about protein interactions in cells, however, these methodologies are also prone to false positives. The protein–protein interface can also be characterized by in-cell NMR. However, quantification of the equilibrium thermodynamics of complex stability is challenging in cells. The few reports tend to involve heterodimerization (20), which can be complicated to assess because the concentration of both reactants must be controlled, fluorescence-resonance-energy transfer because labels adding hundreds to thousands of daltons must be included, or because competition with natural, unlabeled proteins in cells must be considered (21–27).

Results

We use the simplest type of complex and a label that adds only a few Da. The homodimer formed by the A34F variant of the 6.2-kDa domain of protein G (GB1, Fig. 1*A*) is well characterized in buffer (28) and under crowded conditions (18, 29). Both the monomer and dimer are folded, and dimerization involves neither a significant conformational change nor a large reduction in surface area. The effect of surface charge has also been assessed in vitro (30). Importantly, GB1 is not found in these cells, and its diffusion in cells is like other monomeric proteins (31–34), which suggests that fortuitous-competing specific interactions with endogenous proteins are unlikely.

To gain broadly applicable information, we assessed complex stability in a prokaryote (*E. coli*) and a eukaryote (*Xenopus laevis* oocytes). To detect dimerization, we used simple fluorine-labeling techniques and ^{19}F NMR, which is advantageous for studying sensitive living cells because acquisition of spectra requires only a few minutes. Replacing a side chain hydrogen atom with a fluorine adds only 18 Da and has a small or negligible effect on structure and stability. Furthermore, the rate of exchange between the GB1 monomer and dimer is much less than the

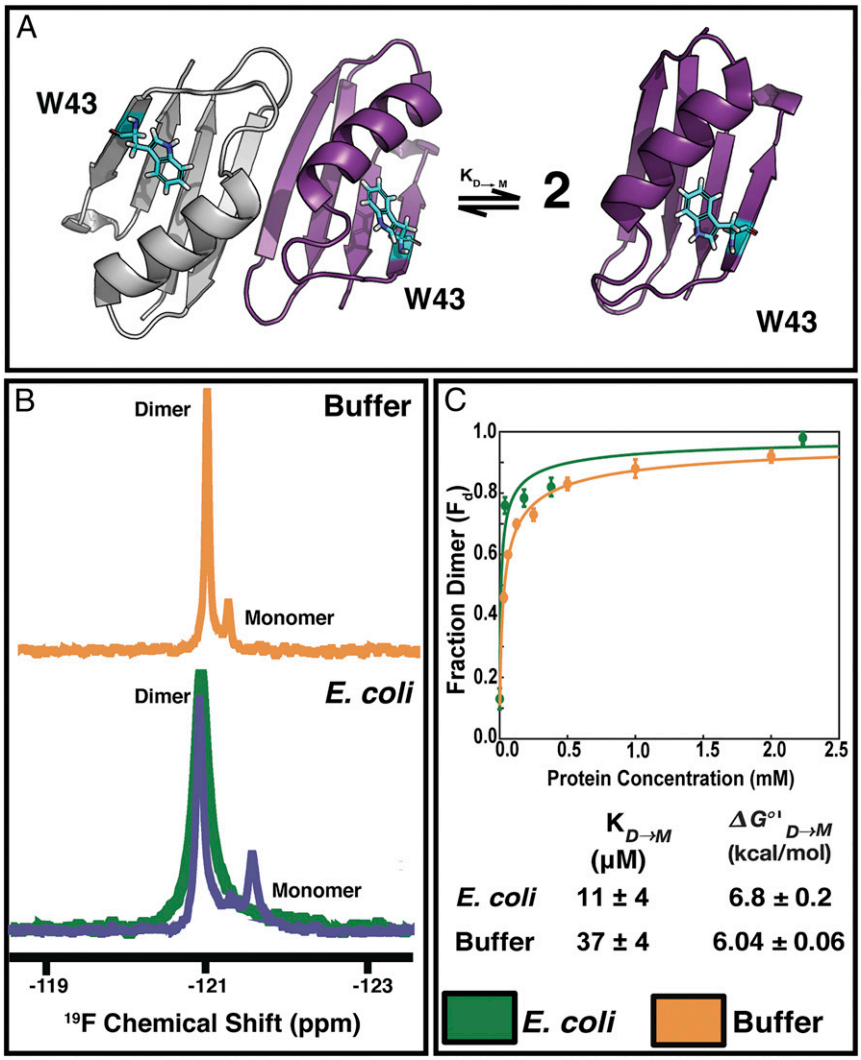

Fig. 1. Complex formation in *E. coli*. (*A*) Dissociation of the A34F GB1 side-by-side homodimer (Protein Data Bank [PDB] ID code 2RMM) showing the tryptophan at position 43. (*B*) ^{19}F NMR spectra acquired at 298 K 6-fluorotryptophan–labeled protein in dilute solution 0.50 mM GB1 in 20 mM phosphate buffer (pH 7.5) and *E. coli* using inducer concentrations of 1.0 mM (green) and 0.24 mM (purple), with the cytosol buffered at pH 7.6. (*C*) Dissociation constants were quantified from the binding isotherms acquired in cells (green) and buffer (orange). Error bars represent the standard deviation of the mean from triplicate analysis.

frequency difference between their resonances, which means that monomer and dimer concentrations are directly proportional to the area of their resonances (28). For studies in *E. coli*, the sole tryptophan of GB1 was replaced by 6-fluorotryptophan (35). For studies in oocytes, its three tyrosines were replaced by 3-fluorotyrosine (31). These two labeling strategies were used because they provide the highest quality data in the two different cell types.

To quantify dimer formation, we measured the fraction of GB1 dimer as obtained from integration of the ^{19}F resonances, as a function of GB1 concentration. These binding isotherms (Figs. 1*C* and 2*C*) were fit to Eq. 1 (36), where F_d is the fraction of dimer and P_t is the total GB1 concentration in cells or in buffer alone to yield the equilibrium dissociation constant, $K_{D\rightarrow M}$ (*SI Appendix*, Figs. S1 and S2).

$$F_d = \frac{4P_t + K_{D\rightarrow M} - \sqrt{K_{D\rightarrow M}^2 + 8P_tK_{D\rightarrow M}}}{4P_t}. \quad [1]$$

Stability is defined as the free energy of homodimer dissociation, $\Delta G^{o'}_{D\rightarrow M} = -RTln(K_{D\rightarrow M})$, where R is the gas constant in kcal/(mol*K) and T is the absolute temperature. Uncertainties are represented as the standard deviation of mean from triplicate measurements. The stability in buffer alone was determined as described (29).

To assess dimerization in *E. coli* (Fig. 1*A*), GB1-expressing plasmids were transformed into a strain containing the Δ*lacZY* mutation to assure tunable control of protein expression GB1 (37), the protein was labeled by adding 6-fluoroindole to the medium (18). Leakage was tested (38) after each experiment. None was observed (37, 39) (*SI Appendix*, Fig. S3). The ^{19}F resonances from the monomer and dimer (Fig. 1*B*) are broader in cells than in buffer (Fig. 1*B*) due to attractive interactions between the GB1 and other cytosolic proteins and the slightly increased viscosity in cells (31–34), but there is no overlap between monomer and dimer in cells (*SI Appendix*, Fig. S4). Quantification of populations requires complete recovery of longitudinal magnetization, which was accomplished with a 4-s delay between acquisitions. Monomer and dimer resonances were fully resolved, and only a few Hz of line broadening was applied prior to Fourier transformation. The GB1 concentration was varied by using different inducer concentrations (37) (*SI Appendix*, Fig. S5). Mass

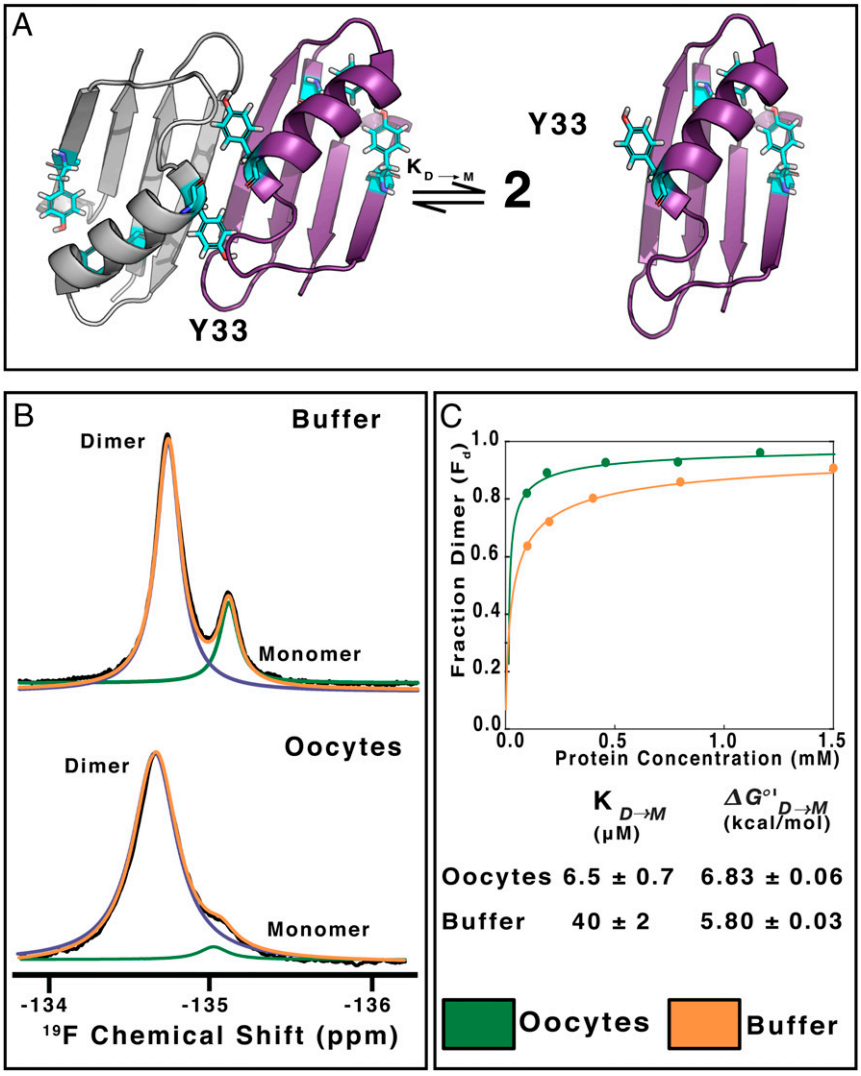

Fig. 2. Complex formation in *X. laevis* oocytes. (*A*) Dissociation of the A34F GB1 side-by-side homodimer (PDB ID code 2RMM) showing the tyrosines at positions 3, 33, and 45. (*B*) ^{19}F NMR spectra acquired at 288 K of the 3-fluorotyrosine–labeled protein in 20 mM phosphate buffer (pH 7.4) and oocytes (black, as acquired; purple, deconvoluted dimer; green, deconvoluted monomer; and orange, sum of deconvolutions). (*C*) Dissociation constants were quantified from binding isotherms acquired in oocytes (green) and buffer (orange). The uncertainties, which are from least squares fitting, are smaller than the points.

spectrometry combined with flow cytometry was used to assess P_t (39). The NMR and protein concentration data were combined to construct binding isotherms (Fig. 1*C*), which were used to determine $\Delta G^{o'}_{D\rightarrow M}$ by least square fitting.

For *X. laevis* oocytes experiments, we microinjected purified ^{15}N-enriched, 3FY-labeled A34F proteins (Fig. 2*A*) along with a proteinase inhibitor mixture to prevent degradation, and recorded ^{19}F spectra (Fig. 2*B*) and ^{15}N–^{1}H heteronuclear single quantum coherence (HSQC) spectra (*SI Appendix*, Fig. S6). The internal pH of oocytes is 7.4 (40). The similarity of spectra acquired in oocytes to those acquired in buffer alone at the same pH (*SI Appendix*, Fig. S6) suggests that the structures are unchanged. As noted in ref. 32, resonances are broader in oocytes than in buffer but not as broad as in *E. coli*. After each in-cell NMR experiment, the supernatant was reexamined by NMR. No leakage was observed (*SI Appendix*, Fig. S7). One-dimensional ^{15}N–^{1}H HSQC spectra acquired before and after acquisition are nearly identical (*SI Appendix*, Fig. S7), indicating that the dimer and monomer concentration is constant in oocytes throughout the experiment. We used a combination of NMR and microscopy to determine P_t (*SI Appendix*, Fig. S8). The concentration of GB1 in the NMR tube was obtained by reference to a sample of known concentration in buffer alone (6). We used a microscope to measure an average oocyte volume of 1.0 ± 0.2 μL (*SI Appendix*, Fig. S8), consistent with another report (41). P_t is the product of average volume and the number of oocytes used in the NMR experiment. To facilitate integration, ^{19}F spectra were fitted to Lorentzian line shapes after Fourier transformation (Fig. 2*B*). The combined results used to construct binding isotherms (Fig. 2*C*) were used to determine $\Delta G^{o'}_{D\rightarrow M}$ by least square fitting. A complete list of $K_{D\rightarrow M}$ and $\Delta G^{o'}_{D\rightarrow M}$ values acquired in *E. coli*, oocytes, and buffer is given in *SI Appendix*, Table S1.

The interior of both *E. coli* cells and oocytes stabilize the A34F dimer relative to buffer (Figs. 1*C* and 2*C*). Such stabilization was initially surprising because the cytoplasm of both prokaryotic and eukaryotic cells usually destabilizes globular proteins (4). Any small differences between intracellular pH and the buffered dilute solutions cannot explain the stability difference because dimer stability changes only by ∼0.1 kcal/mol between pH 6.2 and 7.5 (30), and the stability of GB1 is insensitive to physiologically relevant ionic strengths (42). We suggest that the stabilization in cells arises mostly from repulsive chemical interactions between the client protein and the cellular milieu.

The idea that increased dimer stability in cells arises from hard-core repulsions seems unlikely for two reasons. First, we know from in vitro crowding studies that the A34F variant is nearly insensitive to hard-core repulsive effects (18). Second, if we interpret the results using simple traditional theories and bear in mind that *E. coli* cells are more crowded than oocytes (6), the expectation is that the dimer would be more stable in *E. coli*, but the opposite is true. This analysis suggests that chemical interactions play a key role in protein complex stability in cells, and specifically, the stabilizing effect in both cell types arises from the repulsion between A34F protein, which has a formal charge of −4 in cells and the overall net-negative formal charge on the intracellular proteins (7, 43).

To test the role of electrostatic interactions between GB1 and the cellular milieu, we studied variants that alter the surface charge, comparing their stabilities to that of the A34F protein in buffer (i.e., $\Delta\Delta G^{o'}_{D\rightarrow M} = \Delta G^{o'}_{D\rightarrow M,variant,buffer/cells} - \Delta G^{o'}_{D\rightarrow M,A34F,buffer}$, Fig. 3). The A34F;D40N variant is less anionic (−3 formal charge) than wild-type A34F. Two of the variants A34F;K10N and A34F;N37D are more anionic (−5 formal charge) than wild-type A34F GB1. The estimated net formal charge, on each protein at physiologically relevant pH values is shown at the top of Fig. 3. The changes are all in loops (28) and are expected to have a small effect on structure. Inspection of ^{15}N–^{1}H HSQC acquired in buffer (*SI Appendix*, Figs. S9 and S10) confirm this expectation. For certain variants, only the monomer or dimer is observed in cells (*SI Appendix*, Figs. S11 and S12). For these proteins, we used the minimum or maximum detectable stability (*SI Appendix*, Table S1) to estimate the minimum magnitude of $\Delta\Delta G^{o'}_{D\rightarrow M}$ in Fig. 3. Therefore, the actual positive and negative values of $\Delta\Delta G^{o'}_{D\rightarrow M}$ are larger and smaller than the estimated values, respectively.

First, we consider $\Delta\Delta G^{o'}_{D\rightarrow M}$ in buffer. Both 6FW- and 3FY-labeled proteins (orange and gray bars, respectively) show the same trends, indicating that it is reasonable to compare the differently labeled proteins. Based on charge, two of the three variants behave as anticipated. For A34F;D40N, the decrease in charge–charge repulsions between monomers compared to A34F (−4 to −3), increases dimer stability. For A34F;K10N, the increase in repulsions between monomers (−4 to −5) decreases stability. Contrary to this simple idea, A34F;N37D (also −4 to −5) is more stable than A34F, but the side chain of residue 37 is near the dimer interface (28), so there may be slight perturbations to structure.

Discussion

The behavior of the charge–change variants in both *E. coli* cells and oocytes is consistent with fact that most cellular proteins possess a net negative charge (7, 43). Specifically, if charge–charge interactions are important, we expect that the more negative the charge on the homodimer, the stronger the intermolecular repulsion in cells and the more stable the complex. This prediction is borne out by the data for both cell types, even though some of the stabilities cannot be quantified because only the dimer or monomer is observed. Furthermore, the increased stability in oocytes occurs despite the fact that the g/L protein concentration in oocytes is only about half that of *E. coli* (6). These observations show that chemical interactions are a key determinant of protein behavior in cells.

We can also integrate our knowledge about protein—and protein complex—stability in cells by considering the shapes of the products and reactants. Early expectations for protein stability were based on ideas that globular proteins should be stabilized under crowded conditions because the native state occupies less space than the unfolded state. The validity of these ideas, however, depends in some sense on treating both states as hard, sphere-like objects, which is certainly not the case for the unfolded state. Unfolding proteins also exposes sites for attractive interactions such as hydrogen bonding and hydrophobic contacts, which lead to destabilization. For protein–protein interactions, such as the one studied here, both the reactants and products can be considered more like hard objects such that attractive and repulsive interactions can be more simply rationalized. This is further supported by a recent study showing the A34F variant is barely affected by hard-core repulsions in dilute buffer (18). Perhaps the strongest pieces of evidence for the importance of charge–charge interactions in cells are that all the charge–change variants have essentially the same excluded volume yet show different behaviors in cells, and the fact that simple excluded volume arguments only predict increases in stability under crowded conditions, yet the A34F;D40N variant is less stable in cells than it is in buffer. A34F;D40N may be less stable in *E. coli* cells because it is less anionic and therefore may experience more attractive chemical interactions.

Protein–protein interactions allow cells to respond to chemical and physical stimuli, but nonspecific interactions in the crowded cellular interior inevitably compete with specific interactions and interfere with signal transduction. Protein surface charge plays a determinant role for protein diffusion in cells due to nonspecific interactions within the cytoplasm (33, 34, 44, 45). Our study shows that increasing the negative charge on a protein complex can enhance a specific protein–protein interaction. The data also

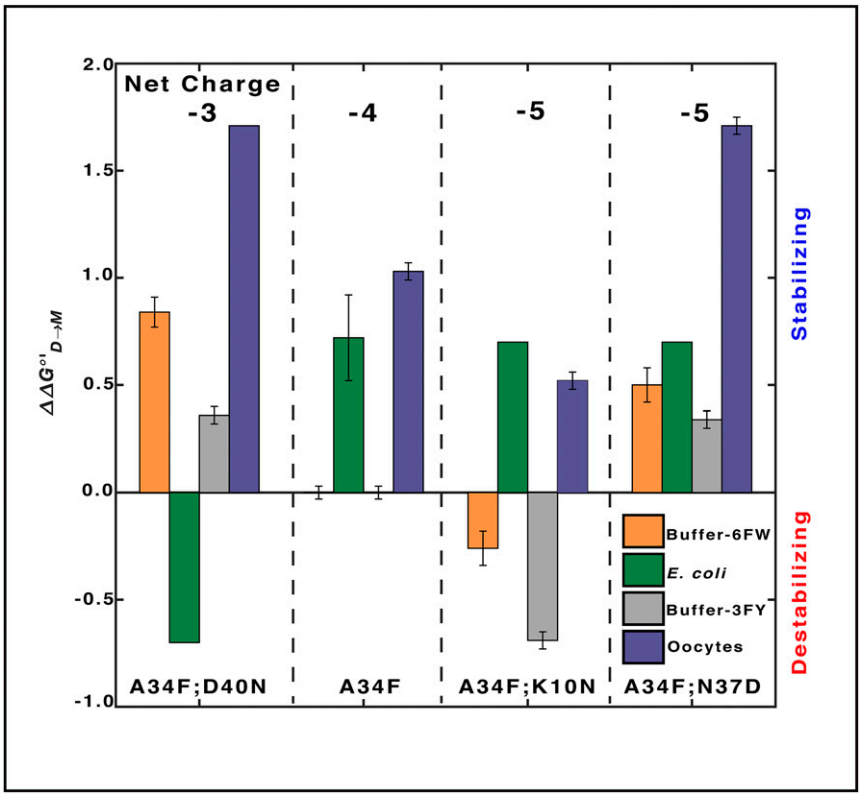

Fig. 3. Charge and dimer stability ($\Delta\Delta G^{o'}_{D\rightarrow M} = \Delta G^{o'}_{D\rightarrow M,variant,buffer/cells} - \Delta G^{o'}_{D\rightarrow M,A34F,buffer}$). Positive values indicate increased stability and vice versa. Uncertainties are propagated from the uncertainties in $\Delta G^{o'}_{D\rightarrow M}$. The absence of error bars indicates minimum magnitude of $\Delta\Delta G^{o'}_{D\rightarrow M}$ for variants exhibiting only dimer or monomer in cells.

suggest a reason why posttranslational modifications such as methylation, acetylation, and protein phosphorylation, which temper positive charge or add negative charge, are used to control signaling. Charge–charge interactions are also important for proper protein function. For instance, a single surface-charge change causes sickle cell disease (46) and myoglobin surface charge correlates with diving ability in mammals (47), and the charge on the loops regions in crystallin are key to eye lens formation (48). Therefore, investigating how the cellular environment tunes specific protein–protein interactions is crucial to advancing our physical understanding of biology and human health.

Materials and Methods

Plasmids. pET-11a harboring the gene for the T2Q;A34F mutant of GB1 was used as the basis of the project. The T2Q change prevents N-terminal degradation (49), and the A34F change causes dimer formation (28). The proteins discussed here carry both changes. Agilent Quick-Change kits or gene synthesis (Gene Universal) was used to construct other mutants.

6FW-Labeled Protein. Protein was expressed and purified as described (29). Briefly, a 1-L culture *E. coli* strain BL21 (DE3) harboring a GB1 construct was grown in ampicillin-containing (100 μg/L final concentration) ^{15}N-enriched M9 media (6.78 g/L Na_2HPO_4, 3 g/L KH_2PO_4, 0.5 g/L NaCl, 1 g/L $^{15}NH_4Cl$, 4 g/L D-glucose, 2 mM $MgSO_4$, 1 mM $CaCl_2$, and 1 mM ampicillin) with shaking at 37 °C at 225 rpm (New Brunswick Scientific, Innova I26). When the cells reached an optical density at 600 nm (OD_{600}) of 0.6 to 0.8, 1 g *N*-(phosphonomethyl)glycine, 60 mg phenylalanine, and 80 mg tyrosine were added. Next, 60 mg 6-fluoroindole (6-FI; Sigma-Aldrich) was dissolved in 250 μL dimethyl sulfoxide (DMSO) and added. After shaking for an additional 45 min, protein expression was induced with isopropyl β-D-1-thio-galactopyranoside (IPTG) at a final concentration of 1 mM.

After 2 h, the cells were pelleted at 4,000 × *g* for 30 min. The supernatant was discarded, and the cells were lysed by sonication (Fisher Scientific Sonic Dismembrator model 500, 15% amplitude, 10 min, 0.50 s on, and 0.50 s off) in 30 mL of 20 mM Tris (pH 7.5) containing protease inhibitor (Roche, cOmplete, EDTA-free inhibitor mixture). The lysate was centrifuged at 15,000 × *g* for 45 min to remove cell debris. The supernatant was filtered (0.45 μm) and loaded on a 16 mm × 25 mm Q Sepharose anion exchange column attached to a GE ÄKTA FPLC. Protein was eluted over a 0 to 50% linear gradient of 20 mM Tris (pH 7.5) to 20 mM Tris, 2 M NaCl (pH 7.5) at 277 K. Fractions were assessed using sodium dodecyl sulfate polyacrylamide gel electrophoresis (SDS-PAGE) with Coomassie blue staining. Fractions containing GB1 were concentrated using a 3,000 Da Amicon centrifugal concentrator. The concentrated sample was loaded on a 16 mm × 600 mm GE Superdex-75 size exclusion column and eluted with M9 salts (3 mM Na_2HPO_4, 2 mM KH_2PO_4, 9 mM NaCl, and pH 7.5 at 277 K).

Purified fractions containing GB1 were concentrated using a 3,000 Da cutoff Amicon centrifugal concentrator and buffer exchanged into sterilized deionized H_2O (18-MΩ). Protein concentration was quantified using a NanoDrop One Spectrophotometer (Thermo Fisher) and an extinction coefficient of 9,970 L M^{-1} cm^{-1} (50). Purified protein was split into 500 μM aliquots, lyophilized for 12 to 16 h and stored at −20 °C. Protein was resuspended in 20 mM sodium phosphate buffer (pH 7.5) containing 10% D_2O for NMR experiments.

3FY-Labeled Protein. ^{15}N-enriched, 3FY-labeled protein was prepared as described (32, 51). Briefly, a single colony of *E. coli* strain BL21 (DE3) containing the appropriate GB1-harboring plasmid was inoculated in 10 mL Luria Broth (LB) media (10 g/L tryptone, 5 g/L yeast extract, 10 g/L NaCl, and 1 mM ampicillin). The culture was shaken overnight at 37 °C and transferred to 100 mL tryptone-yeast media (16 g/L tryptone, 10 g/L yeast extract, 5 g/L NaCl, 1 mM NaOH, and 1 mM ampicillin). After 2 h of shaking at 37 °C, the cells were centrifuged, and the pellet resuspended in 1 L ^{15}N-enriched M9 media and shaken at 37 °C. When the cells reached an OD_{600} of 0.4, 0.5 g glyphosate, 70 mg 3-fluorotyrosine, 60 mg tryptophan, and 60 mg phenylalanine were added. The culture was then grown to an OD_{600} of 0.6, and protein expression was induced with IPTG at a final concentration of 1 mM. After 2 h, the pellet was collected by centrifugation at 6,000 rpm (JA-10 rotor, Beckman coulter) for 10 min and stored at −20 °C.

The pellet was resuspended in 20 mM Tris, pH 7.5, sonicated (Scientz-IID JY92-IIN, 40% amplitude, 30 min, 3 s on, and 6 s off), and then centrifuged for 30 min at 20,000 rpm (JA-25.5 rotor, Beckman coulter). The supernatant was loaded on a 16 mm × 100 mm anion exchange column (GE HiPrep DEAE FF 16/10) attached to a GE ÄKTA FPLC. The protein was eluted with a gradient from 0 to 1 M NaCl. The fractions were assessed by SDS-PAGE with Coomassie staining. GB1-containing fractions were concentrated using a 3,000-molecular-weight–cutoff Amicon centrifuge filter and loaded on a 26 mm × 600 mm GE Superdex-100 size exclusion column equilibrated with 20 mM Tris, 250 mM NaCl, and pH 7.5 at 277 K. GB1-containing fractions were exchanged into triply distilled H_2O (1.5 MΩ cm) by using a desalting column (GE HiPrep 26/10, Sephadex G-25F). Purity was assessed by SDS-PAGE with Coomassie staining. Pure GB1-containing fractions were concentrated and buffer exchanged into sterilized deionized H_2O. Protein concentration was quantified at 280 nm as described above. The purified protein was lyophilized (Alpha 1–4 LD plus, Martin Christ) and stored at −20 °C. Dimer stability in buffer was assessed as described (29).

***E. coli* In-Cell Spectra.** Samples were prepared as described (37). Briefly, a plasmid containing the gene for a GB1 variant was transformed into Tuner (DE3) cells (Novagen) by heat shock. A single colony was used to inoculate 5 mL LB media supplemented with 100 μg/L ampicillin. After the culture was shaken at 37 °C at 225 rpm for 6 to 8 h, 500 μL was used to inoculate 100 mL M9 media. The 100 mL culture was incubated with shaking at 37 °C overnight and added to 100 mL fresh M9 media. The culture was incubated at 37 °C. When the OD_{600} reached between 0.6 and 0.8, 12 mg 6-FI dissolved in 250 μL DMSO was added. After shaking for an additional 45 min, IPTG was added to induce protein expression. After 45 min, 50 μg/L chloramphenicol was added to halt protein expression.

Three 1-mL aliquots were taken from the in-cell culture for liquid chromatography mass spectrometry to determine protein concentration (39). The cells were pelleted at 2,000 × *g* for 20 min and washed three times with an in-cell NMR buffer (200 mM Hepes and 100 mM bis-Tris propane dissolved in 10% D_2O, pH 7.6). The pellet was resuspended in 250 μL in-cell NMR buffer. To check for leakage, after each in-cell spectrum, the sample was gently pelleted, and a spectrum of the twofold diluted supernatant was acquired. No leakage was observed. Example supernatant samples were similar to those reported by Chu et al. (37).

***E. coli* In-Cell HSQC Spectra.** Samples were prepared as described above (37). A single colony from the transformed into Tuner (DE3) cells was used to inoculate 50 mL LB media supplemented with 100 μg/L ampicillin. After shaking at 37 °C at 225 rpm for 6 to 8 h, the cells were pelleted at 2,000 × *g* (Sorvall ST 16 Centrifuge) for 10 min. The pellet was then resuspended with 200 mL M9 media containing 1 g/L $^{15}NH_4Cl$ as the sole nitrogen source. The culture was incubated at 37 °C. When the OD_{600} reached 0.8, 12 mg 6-FI dissolved in 250 μL DMSO was added. The culture was shaken until an OD_{600} of 1.2 was reached whereupon 1 mM IPTG (final concentration) was added to induce protein expression. After 3 h, 50 μg/L chloramphenicol was added to halt protein expression. The cells were pelleted at 2,000 × *g* for 10 min. The pellet was resuspended in 250 μL M9 with 10% D_2O (pH 7.5). Leakage was assessed as described above. No leakage was observed.

Preparing *X. laevis* Oocytes. Oocytes were prepared as described (52). Briefly, ovary lobes were surgically removed to ND96-Ca^{2+} buffer (96 mM NaCl, 2 mM KCl, 1 mM $MgCl_2$, 5 mM Hepes, and pH 7.4). After washing, the ovaries were digested with collagenase (2 mg/mL final concentration). Oocytes were then washed in ND96 (96 mM NaCl, 2 mM KCl, l mM $MgCl_2$, 5 mM Hepes, and pH 7.4) and then ND96 containing 1.8 mM $CaCl_2$. Stage-VI oocytes were selected for microinjection. The protein solution, about 40 nL containing 30% vol/vol P1860-protease inhibitor mixture (Sigma-Aldrich), was injected into each oocyte via an IM-300 microinjector (Narishige Co. Ltd.). About 100 oocytes in ND96 buffer containing 10% D_2O were transferred to a Shigemi micro-NMR tube.

In Vitro Spectra of 6FW-Labeled Proteins. ^{19}F spectra were acquired at 298 K on a 500 MHz Bruker Avance III HD spectrometer equipped with a QCI cryogenic probe. Data were analyzed using TopSpin 3.6.1. Spectra comprised 32,768 points, 512 scans, an acquisition time of 0.9 s, and a sweep width of 20 ppm. The ^{15}N–^{1}H HSQC spectra comprised of 2,048 points ^{15}N and 128 points ^{1}H, 64 scans, an acquisition time of 0.12 s for ^{15}N and 0.02 s for ^{1}H, and a sweep width of 44 ppm for ^{15}N and 13 ppm for ^{1}H. Data were processed with nmrPipe and NMRViewJ. The spectra were acquired in 200 mM Hepes, 100 mM bis-Tris propane, 150 μg/mL ampicillin, and 50 μg/mL chloramphenicol in 10% D_2O (pH 7.6). The GB1 concentration was varied from 20 μM to 2 mM.

In-Cell HSQC Spectra of 6FW-Labeled Proteins. ^{15}N–^{1}H HSQC spectra were acquired at 298 K on a 600 MHz Bruker Avance III HD spectrometer. Data were analyzed using TopSpin 3.6.2. Spectra comprised of 2,048 points ^{15}N and 128 points ^{1}H, 32 scans, an acquisition time of 0.12 s for ^{15}N and 0.02 s for ^{1}H, and a sweep width of 44 ppm for ^{15}N and 13 ppm for ^{1}H. Data were processed with nmrPipe and NMRViewJ. The spectra were acquired in M9 media containing 50 μg/mL chloramphenicol and 10% D_2O (pH 7.5). The GB1 concentration was 2 mM.

NMR of 3FY-Labeled Proteins. Experiments were performed at 288 K on a 600 MHz spectrometer (Bruker) equipped with H/F/(C, N) triple-resonance cryogenic probe. ^{19}F spectra were acquired with a sweep width 11.31 kHz, a relaxation delay 2.5 s, and an acquisition time of 1.45 s. The number of pulses was 1,024. The spectral width of 1D ^{15}N–^{1}H HSQC spectra was 16 ppm for ^{1}H. The relaxation delay was 1.5 s, the acquisition time was 0.11 s, and number of pulses was 512. For ^{15}N–^{1}H HSQC, the spectral width was 16 ppm for ^{1}H and 40 ppm for ^{15}N. The relaxation delay was 1.5, acquisition time was 0.11 s, and the number of pulses per increment was 16. The spectra were acquired in 20 mM sodium phosphate in 10% D_2O at pH 7.4. The GB1 concentration varied from 50 μM to 1.5 mM.

Data Analysis in Oocytes. Data were analyzed using TopSpin 3.6.1 or 3.2 with line-broadening of ^{19}F and one-dimensional ^{15}N–^{1}H HSQC spectra of 4.0 Hz and 0.3 Hz, respectively. Peak fitting of ^{19}F spectral and the area of dimer and monomer peak was accomplished with Topspin or OriginPro 8.5.1. Relative populations of dimer and monomer were obtained via integration. The fraction of dimer (F_d) was calculated by dividing the integral of the dimer peak by the sum of the integrals of the monomer and dimer peaks. Data were fit to Eq. 1 using MATLAB (R2020A) or Origin.

Data Availability. All study data are included in the article and/or *SI Appendix*.

ACKNOWLEDGMENTS. We thank Gregory Young and Stu Parnham for spectrometer maintenance, Brandie Ehrmann for help with mass spectrometry, Jeffrey Bonin for help with NMR data processing, and Elizabeth Pielak for comments on the manuscript. This work was supported by the NSF (MCB-1410854 to G.J.P.), the NIH (R01GM127291 to G.J.P.), the Ministry of Science and Technology of China (2017YFA0505400 to C.L. and 2018YFE0202300 to M.L.), the National Natural Science Foundation of China (21925406, 21921004 to C.L. and 21991080 to M.L.) and some of the data were acquired in facilities at the University of North Carolina supported by the National Cancer Institute (P30 CA016086) and the NSF (CHE-1726291). S.L.S., I.-T.C., and A.J.G. were also supported by the NIH (T32 GM008570) and A.J.G. also received support from the NIH (F31 GM126763).

1. Q. Cong, I. Anishchenko, S. Ovchinnikov, D. Baker, Protein interaction networks revealed by proteome coevolution. *Science* **365**, 185–189 (2019).
2. N. Sahni *et al*., Widespread macromolecular interaction perturbations in human genetic disorders. *Cell* **161**, 647–660 (2015).
3. K. E. van Holde, *Physical Biochemistry* (Prentice Hall, 1985).
4. A. J. Guseman, G. J. Pielak, "Protein stability and weak intracellular interactions" in *In-Cell NMR Spectroscopy: From Molecular Sciences to Cell Biology*, Y. Ito, V. Dötsch, M. Shirakawa, Eds. (The Royal Society of Chemistry, 2019), pp. 188–206.
5. S. B. Zimmerman, S. O. Trach, Estimation of macromolecule concentrations and excluded volume effects for the cytoplasm of *Escherichia coli*. *J. Mol. Biol.* **222**, 599–620 (1991).
6. F.-X. Theillet *et al*., Physicochemical properties of cells and their effects on intrinsically disordered proteins (IDPs). *Chem. Rev.* **114**, 6661–6714 (2014).
7. L. P. Kozlowski, Proteome-pI: Proteome isoelectric point database. *Nucleic Acids Res.* **45**, D1112–D1116 (2017).
8. E. H. McConkey, Molecular evolution, intracellular organization, and the quinary structure of proteins. *Proc. Natl. Acad. Sci. U.S.A.* **79**, 3236–3240 (1982).
9. R. D. Cohen, G. J. Pielak, A cell is more than the sum of its (dilute) parts: A brief history of quinary structure. *Protein Sci.* **26**, 403–413 (2017).
10. V. Pareek, H. Tian, N. Winograd, S. J. Benkovic, Metabolomics and mass spectrometry imaging reveal channeled de novo purine synthesis in cells. *Science* **368**, 283–290 (2020).
11. M. Sarkar, C. Li, G. J. Pielak, Soft interactions and crowding. *Biophys. Rev.* **5**, 187–194 (2013).
12. P. R. Davis-Searles, A. J. Saunders, D. A. Erie, D. J. Winzor, G. J. Pielak, Interpreting the effects of small uncharged solutes on protein-folding equilibria. *Annu. Rev. Biophys. Biomol. Struct.* **30**, 271–306 (2001).
13. C. B. Anfinsen, Principles that govern the folding of protein chains. *Science* **181**, 223–230 (1973).

14. D. Chakravarty, M. Guharoy, C. H. Robert, P. Chakrabarti, J. Janin, Reassessing buried surface areas in protein-protein complexes. *Protein Sci.* **22**, 1453–1457 (2013).
15. K. A. Sharp, Analysis of the size dependence of macromolecular crowding shows that smaller is better. *Proc. Natl. Acad. Sci. U.S.A.* **112**, 7990–7995 (2015).
16. F. Zosel, A. Soranno, K. J. Buholzer, D. Nettels, B. Schuler, Depletion interactions modulate the binding between disordered proteins in crowded environments. *Proc. Natl. Acad. Sci. U.S.A.* **117**, 13480–13489 (2020).
17. A. P. Minton, Excluded volume as a determinant of macromolecular structure and reactivity. *Biopolymers* **20**, 2093–2120 (1981).
18. A. J. Guseman, G. M. Perez Goncalves, S. L. Speer, G. B. Young, G. J. Pielak, Protein shape modulates crowding effects. *Proc. Natl. Acad. Sci. U.S.A.* **115**, 10965–10970 (2018).
19. E. J. Deeds, O. Ashenberg, J. Gerardin, E. I. Shakhnovich, Robust protein protein interactions in crowded cellular environments. *Proc. Natl. Acad. Sci. U.S.A.* **104**, 14952–14957 (2007).
20. S. S. Stadmiller, G. J. Pielak, Protein-complex stability in cells and *in vitro* under crowded conditions. *Curr. Opin. Struct. Biol.* **66**, 183–192 (2020).
21. X. You *et al*., Intracellular protein interaction mapping with FRET hybrids. *Proc. Natl. Acad. Sci. U.S.A.* **103**, 18458–18463 (2006).
22. T. Sudhaharan *et al*., Determination of in vivo dissociation constant, K_D, of Cdc42-effector complexes in live mammalian cells using single wavelength fluorescence cross-correlation spectroscopy. *J. Biol. Chem.* **284**, 13602–13609 (2009).
23. Y. Phillip, V. Kiss, G. Schreiber, Protein-binding dynamics imaged in a living cell. *Proc. Natl. Acad. Sci. U.S.A.* **109**, 1461–1466 (2012).
24. S. Sukenik, P. Ren, M. Gruebele, Weak protein-protein interactions in live cells are quantified by cell-volume modulation. *Proc. Natl. Acad. Sci. U.S.A.* **114**, 6776–6781 (2017).
25. D. Guin, M. Gruebele, Chaperones Hsc70 and Hsp70 bind to the protein PGK differently inside living cells. *J. Phys. Chem. B* **124**, 3629–3635 (2020).
26. M. Jiao, H.-T. Li, J. Chen, A. P. Minton, Y. Liang, Attractive protein-polymer interactions markedly alter the effect of macromolecular crowding on protein association equilibria. *Biophys. J.* **99**, 914–923 (2010).
27. Y. Yang *et al*., In-cell destabilization of a homodimeric protein complex detected by DEER spectroscopy. *Proc. Natl. Acad. Sci. U.S.A.* **117**, 20566–20575 (2020).
28. J. Jee, I.-J. L. Byeon, J. M. Louis, A. M. Gronenborn, The point mutation A34F causes dimerization of GB1. *Proteins* **71**, 1420–1431 (2008).
29. A. J. Guseman, G. J. Pielak, Cosolute and crowding effects on a side-by-side protein dimer. *Biochemistry* **56**, 971–976 (2017).
30. A. J. Guseman, S. L. Speer, G. M. Perez Goncalves, G. J. Pielak, Surface charge modulates protein-protein interactions in physiologically relevant environments. *Biochemistry* **57**, 1681–1684 (2018).
31. Y. Ye *et al*., ^{19}F NMR spectroscopy as a probe of cytoplasmic viscosity and weak protein interactions in living cells. *Chemistry* **19**, 12705–12710 (2013).
32. Y. Ye *et al*., Labeling strategy and signal broadening mechanism of protein NMR spectroscopy in *Xenopus laevis* oocytes. *Chemistry* **21**, 8686–8690 (2015).
33. Y. Ye *et al*., Positively-charged tags impede protein mobility in cells as quantified by ^{19}F NMR. *J. Phys. Chem. B* **123**, 4527–4533 (2019).
34. S. Leeb, F. Yang, M. Oliveberg, J. Danielsson, Connecting longitudinal and transverse relaxation rates in live-cell NMR. *J. Phys. Chem. B* **124**, 10698–10707 (2020).
35. P. B. Crowley, C. Kyne, W. B. Monteith, Simple and inexpensive incorporation of ^{19}F-tryptophan for protein NMR spectroscopy. *Chem. Commun. (Camb.)* **48**, 10681–10683 (2012).
36. J. M. Aramini *et al*., ^{19}F NMR reveals multiple conformations at the dimer interface of the nonstructural protein 1 effector domain from influenza A virus. *Structure* **22**, 515–525 (2014).
37. I.-T. Chu, S. L. Speer, G. J. Pielak, Rheostatic control of protein expression using Tuner cells. *Biochemistry* **59**, 733–735 (2020).
38. C. O. Barnes, G. J. Pielak, In-cell protein NMR and protein leakage. *Proteins* **79**, 347–351 (2011).
39. S. L. Speer, A. J. Guseman, J. B. Patteson, B. M. Ehrmann, G. J. Pielak, Controlling and quantifying protein concentration in *Escherichia coli*. *Protein Sci.* **28**, 1307–1311 (2019).
40. M. F. Cicirelli, K. R. Robinson, L. D. Smith, Internal pH of *Xenopus* oocytes: A study of the mechanism and role of pH changes during meiotic maturation. *Dev. Biol.* **100**, 133–146 (1983).
41. N. Parisis, *Xenopus laevis* as a model-system. *Mater. Methods* **2**, 151 (2012).
42. S. Lindman *et al*., Salting the charged surface: pH and salt dependence of protein G B1 stability. *Biophys. J.* **90**, 2911–2921 (2006).
43. S. Leeb *et al*., Diffusive protein interactions in human versus bacterial cells. *Curr. Res. Struct. Biol.* **2**, 68–78 (2020).
44. X. Mu *et al*., Physicochemical code for quinary protein interactions in *Escherichia coli*. *Proc. Natl. Acad. Sci. U.S.A.* **114**, E4556–E4563 (2017).
45. P. E. Schavemaker, W. M. Śmigiel, B. Poolman, Ribosome surface properties may impose limits on the nature of the cytoplasmic proteome. *eLife* **6**, e30084 (2017).
46. W. A. Eaton, Hemoglobin S polymerization and sickle cell disease: A retrospective on the occasion of the 70th anniversary of Pauling's science paper. *Am. J. Hematol.* **95**, 205–211 (2020).
47. S. Mirceta *et al*., Evolution of mammalian diving capacity traced by myoglobin net surface charge. *Science* **340**, 1234192 (2013).
48. J. Cai, J. P. Townsend, T. C. Dodson, P. A. Heiney, A. M. Sweeney, Eye patches: Protein assembly of index-gradient squid lenses. *Science* **357**, 564–569 (2017).
49. C. K. Smith, J. M. Withka, L. Regan, A thermodynamic scale for the β-sheet forming tendencies of the amino acids. *Biochemistry* **33**, 5510–5517 (1994).
50. S. C. Gill, P. H. von Hippel, Calculation of protein extinction coefficients from amino acid sequence data. *Anal. Biochem.* **182**, 319–326 (1989).
51. C. Li *et al*., Protein ^{19}F NMR in *Escherichia coli*. *J. Am. Chem. Soc.* **132**, 321–327 (2010).
52. Y. Ye, X. Liu, G. Xu, M. Liu, C. Li, Direct observation of Ca^{2+}-induced calmodulin conformational transitions in intact *Xenopus laevis* oocytes by ^{19}F NMR spectroscopy. *Angew. Chem. Int. Ed. Engl.* **54**, 5328–5330 (2015).